Use of Atmospheric Braking During Mars Missions

M. E. Tauber* and J. V. Bowles†
NASA Ames Research Center, Moffett Field, California
and
Lily Yang‡
Sterling Software, Palo Alto, California

For early five-person Mars missions lasting 14 to 16 months, total system weights in low Earth orbit range from 1–2.4 × 10^6 kg. The atmospheric entry velocities at Mars vary from 6.7 to 8.6 km/s. It is shown that a high-lift winged vehicle can use atmospheric braking very effectively to decelerate upon arrival at Mars. Following a nearly-constant-altitude deceleration period, the vehicle is allowed to skip out of the atmosphere and go into a low planetary orbit. For an entry speed of 7.8 km/s, the atmospheric braking period lasts about 10 min with a peak deceleration that could potentially be held below 1.5 Earth *g*. The atmospheric maximum heating rate approached 100 W/cm² at the stagnation point for a fully catalytic surface. The corresponding equilibrium wall temperature was 2150 K. For a partially catalytic wall, the stagnation point, a representative wing leading-edge point, and the windward-surface centerline peak heating was about 40 to 65 W/cm², resulting in wall temperatures of under 2000 K. In fact, the vehicle could be radiatively cooled to an entry speed of over 8 km/s. The total heat loads were roughly comparable to values experienced during Shuttle entry. The combination of high lift and effective modulation of the lift afforded by a winged configuration resulted in an efficient Mars atmospheric braking and surface descent vehicle.

Nomenclature

A = reference area of entry vehicle
a = acceleration
C_D = drag coefficient
D = drag
g = acceleration of gravity
h_∞ = freestream enthalpy
h_{aw} = adiabatic wall enthalpy
h_w = wall enthalpy
H = total enthalpy at boundary-layer edge
L = lift
m = vehicle mass
$\dot{q}_w$ = heat-transfer rate into the body per unit area, W/cm²
R_o = planetary radius
r_n = body nose radius, m
s = distance along trajectory
T_w = equilibrium wall temperature, K
t = time
V = flight velocity, m/s
V_s = surface grazing (circular) satellite speed
W = vehicle weight
x = distance along body surface
α = angle of attack
γ = flightpath angle
Λ = sweepback angle
ρ = freestream density, kg/m³

Subscripts

cyl = cylinder
E = entry condition
FP = flat plate
LE = leading edge
o = stagnation point
ov = overshoot
un = undershoot

Introduction

THE next major step in the manned exploration of the solar system will likely be a mission to Mars. Previous studies[1–3] have shown that large weight and cost savings can be achieved by using atmospheric braking, especially when arriving at Mars, instead of decelerating propulsively. However, a manned interplanetary mission is an extremely complex undertaking that requires study of many technological tradeoffs in diverse disciplines. Among these are such fundamental physiology questions as determining the need for artificial gravity during the long interplanetary voyage, and, if none is used so as to reduce weight and complexity, whether a time limit must be imposed on the duration of manned missions. As shown by Park and Davies,[4] setting very short (330 day) trip time limits can greatly complicate the mission by increasing departure velocity requirements. High departure velocities, in turn, result in high planetary arrival speeds and a much more severe atmospheric braking environment. Additional complexity is introduced if the mission dates are varied and if guidance problems are considered. The optimization of the entire mission is far beyond the scope of this or any other single paper. Therefore, the present paper will be limited to studying the conditions encountered for Mars arrival velocities that are representative of the optimum Earth-Mars alignments occuring every 15 years. To reduce the crew exposure to the hazards of long-duration spaceflight, only so-called "sprint" missions will be considered. These fast missions typically last 14 to 16 months and can result in high-entry velocities. Trajectories using Venus swingbys are not studied, although some weight might be saved,[5] because the solar radiation intensity can be doubled during the swingby maneuver.

The paper begins with a definition of the major mission parameters, including launch weights in Earth orbit, to define a range of realistic planetary entry speeds. Using these entry speeds, atmospheric braking trajectories are calculated with emphasis on achieving low decelerations.

Presented as Paper 89-1730 at the AIAA 24th Thermophysics Conference, Buffalo, NY, June 12–15, 1989; received July 10, 1989; revision received Dec. 11, 1989. Copyright © 1989 American Institute of Aeronautics and Astronautics, Inc. No copyright is asserted in the United States under Title 17, U.S. Code. The U.S. Government has a royalty-free license to exercise all rights under the copyright claimed herein for Governmental purposes. All other rights are reserved by the copyright owner.

*Research Scientist. Associate Fellow AIAA.
†Research Scientist. Member AIAA.
‡Professional Staff Member.

The vehicle aerodynamic characteristics that are required to fly the trajectories are also determined. Lastly, the atmospheric heating, the corresponding equilibrium wall temperatures, and the total heat loads at key body locations are presented and discussed.

Mission Scenario

The next optimum alignment of Earth and Mars will occur in 2003. The planetary departure and entry-conditions characteristics of missions during 2003 were found by using the *Planetary Flight Handbook.*[6] (It was assumed that the 1988 velocity chart was sufficiently accurate for present purposes, since the planetary alignments come very close to repeating every 15 years.) It is necessary to consider actual mission scenarios to identify the range of realistic atmospheric entry conditions. One measure of the realism of the conditions is found by selecting combinations of departure and entry conditions from the charts in Ref. 6 and then estimating the mission total weight requirements. Mission durations were varied from 14 to 16 months, including a 1-month stay on Mars. A five-person crew was assumed, with three crew members descending to the Martian surface. Therefore, the mission discussed here can be considered an early exploratory one. Another objective of the mission is to check the physiological reaction and technological ability to protect humans during prolonged space flights and subsequent planetary landings; thus, a benign crew environment during atmospheric braking and surface landing is highly desirable, and low decelerations are especially important upon arrival at Mars and during landing since the crew is expected to explore the surface. In contrast, after returning to Earth, only minimal physical activity is required and recuperative facilities are available.

Four representative missions lasting 14 to 16 months and having moderate Mars entry speeds were selected from the 1988 (corresponding to 2003) dated chart in Ref. 6. As can be seen from Table 1, the Martian atmospheric inertial entry velocities varied from 6.65 to 8.6 km/s, whereas the corresponding Earth entry speeds ranged from 17 to 15.5 km/s. The orbital launch velocities ranged from 5.70 to 6.95 km/s at Earth and from 6.19 to 7.94 km/s at Mars. The apparently modest variations in the launch velocities required for the four cases can magnify the differences in the initial launch masses in Earth orbit, as will be shown next.

The total initial weight in low Earth orbit was calculated by assuming that atmospheric braking is used at Mars and on return to Earth. For Earth launch, cryogenic propellants are used consisting of liquid oxygen and liquid hydrogen with a specific impulse of 480 s. For Mars departure, the use of storable liquid propellants having a specific impulse of 350 s was assumed. Estimates for the fixed masses are listed in Table 2. It was also assumed that the mass of the tanks, pumps, engines, and other equipment for the cryogenic propellants was 10% of the fuel mass, whereas 7.5% was used for the storable fuels used at Mars. The initial masses required for the four missions, given in Table 3, varied from $1\text{–}2.4 \times 10^6$ kg. Note that of the four missions the one having the largest ΔV for Mars departure requires the maximum mass in Earth orbit. Therefore, the ΔV at Mars departure appears to have a greater effect on mission total mass than an equivalent velocity increment at launch from Earth orbit. [The total masses required for the mission (shown in Table 3) approximate the values given in Refs. 1–3, where missions using solely cryogenic propellants and atmospheric braking at both planets were studied.]

The scenario envisioned here assumes that one or more vehicles are launched from Earth orbit toward Mars. If two vehicles are used, one may carry the crew to Mars whereas the other may contain the Earth return capsule, other equipment, and the propulsion system for the return voyage, for example. Since the primary objective here is to study the atmospheric entry environment at Mars, no additional details or tradeoffs in the mission scenario will be considered.

Table 1 Some missions for the year 2003

Mission time, days	ΔV Earth, km/s	ΔV Mars, km/s	V entry Mars, km/s	V entry Earth, km/s
421	5.70	6.48	8.60	15.5
458	6.95	6.19	7.80	15.4
450	5.70	7.94	8.60	15.7
475	5.70	7.35	6.65	17.0

Table 2 Mass estimates for 2003 missions—fixed masses

Earth atmosphere entry capsule	5,000 kg
Interplanetary living modules	5,000 kg
Consumables (assuming recycling)	20 kg/day
Mars manned atmospheric capture and landing vehicle, including living facilities	15,000 kg
Mars orbital ascent vehicle (minus fuel)	2,000 kg
Power generation and communication equipment	2,500 kg
Heat shielding for freight vehicle	5 kg/m^2

Table 3 Mass estimates for 2003 missions—fuel and mission masses ($\times 10^6$ kg)

Mission time, day	Earth orbit departure fuel	Mars orbit departure fuel	Initial mass in Earth orbit
421	0.695	0.145	0.99
458	1.04	0.123	1.35
450	1.70	0.430	2.42
475	1.09	0.258	1.56

Atmospheric Deceleration and Planetary Capture

The present study will concentrate on the arrival conditions and the atmospheric braking of the manned vehicle at Mars. In Refs. 7 and 8, it was shown that a high-lift winged vehicle was very well suited for making a gliding descent to the Martian surface. When the descent trajectories were initiated from a low Martian orbit at a speed of 3.5 km/s, the peak deceleration loads ranged from 0.7 to 0.9 Earth g. Here the suitability of using a larger manned version of the configuration proposed in Refs. 7 and 8 will be investigated. The proposed manned vehicle is 30 m long, has a nose radius of 0.9 m, and retains the 70 deg wing leading-edge sweep (see Fig. 1). The deceleration of the vehicle within the atmosphere will be studied for entry speeds listed in Table 1, which varied from about 6.7 to 8.6 km/s. When the vehicle has slowed to 3.5 km/s, it is permitted to skip out of the atmosphere and go into a low-altitude planetary orbit. The aerodynamic deceleration load and heating environment encountered by the vehicle during the atmospheric braking pass will be calculated. The atmospheric composition and structure that will be used is based on the Viking Mars lander measurements and is described in Refs. 7 and 8.

Trajectory Parameters

An entry at a speed of 7.8 km/s (the second case shown in Table 1) will be used to illustrate the atmospheric deceleration and planetary capture maneuver. The entry trajectory will be computed for a relative velocity (with respect to the rotating atmosphere) of 7.6 km/s and an entry angle of -7.7 deg at an altitude of 90 km. A 30-deg angle of attack will be used, which will result in an m/C_DA of 500 kg/m^2. The lift will be modulated by rolling the vehicle and thus rotating the lift vector. It is necessary to find trajectories that assure high-speed atmospheric capture during a single pass, since the vehicle enters at hyperbolic speed. Failure to decelerate below the 5 km/s escape velocity during the first pass results in a skip-out into a solar orbit, which is catastrophic. Flight near the overshoot

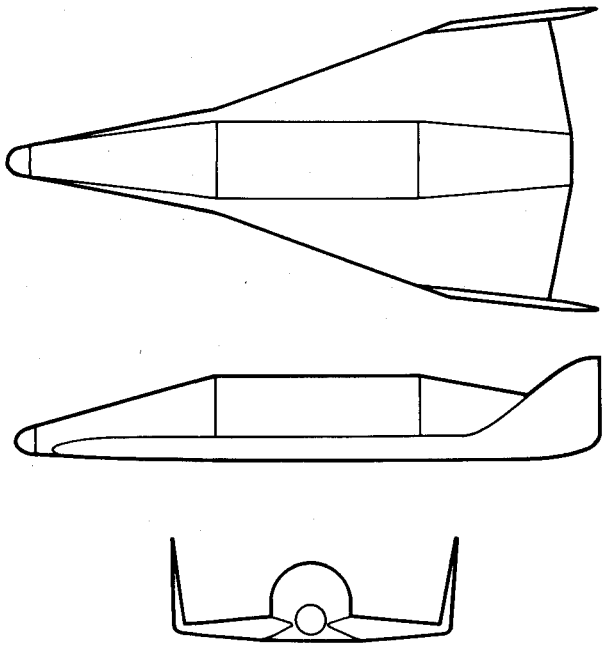

Fig. 1 Three views of proposed vehicle configuration.

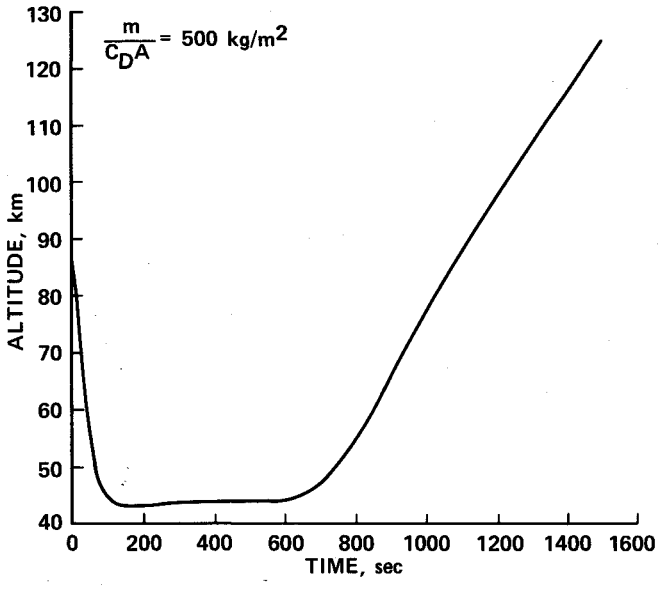

Fig. 2 Variation of relative velocity with time during atmospheric braking.

boundary is considered since the decelerations must be modest for crew safety and the vehicle must skip out at 3.5 km/s into a low planetary orbit. A trajectory that meets these criteria is shown in Figs. 2 and 3, where the variation of altitude and velocity with time are presented. It is noteworthy that most of the deceleration occurs at a roughly constant altitude near 44 km over a period of about 10 min. If an undershoot boundary is defined by assuming a 4-g deceleration limit, then the corridor width is about 3.5 deg of entry angle. A maximum absolute L/D of 0.8 has been used to determine the corridor.

Aerodynamic Requirements and Deceleration Loads

The advantages of using a high-lift configuration for the manned vehicle at Mars become apparent when the guidance requirements to achieve atmospheric capture and to decelerate slowly are considered. To gain physical insight, simplified expressions for the atmospheric overshoot and undershoot boundaries will be derived.

The equations of motion normal and tangential to the flightpath are for unpowered flight in a nonrotating atmosphere[9]

$$L = W\cos\gamma - mV^2\left(\frac{\cos\gamma}{R_o} + \frac{d\gamma}{ds}\right) \tag{1a}$$

and

$$D = W\sin\gamma - m\frac{dV}{dt} \tag{1b}$$

where it is assumed that the flight altitude is much less than the planet's radius R_o. When the flightpath angle approaches zero, Eqs. (1) simplify to

$$L = W - mV^2\left(\frac{1}{R_o} + \frac{d\gamma}{ds}\right) \tag{2a}$$

and

$$D = -m\frac{dV}{dt} \tag{2b}$$

The deceleration force experienced by the vehicle crew can be written as[10]

$$\frac{a}{g} = \frac{dV}{dt}\left(\frac{1}{g}\right)\left[1 + \left(\frac{L}{D}\right)^2\right]^{1/2} \tag{3}$$

where L/D is the lift-to-drag ratio of the vehicle. The overshoot altitude boundary is determined by Eq. (2a) and the acceleration limited undershoot boundary comes from combining Eqs. (2b) and (3). For manned vehicles, the flightpaths are very shallow and the angle should change slowly near the boundaries. Therefore, the first term in parentheses in Eq. (2a) is usually much larger than the second term, which will be neglected to first order. After defining the surface grazing Martian circular satellite velocity as $V_s = (gR_o)^{1/2}$, it is easily shown that the atmospheric density altitude at overshoot is approximately given by

$$\rho_{ov} \approx \frac{2}{R_o}\left(\frac{m}{C_L A}\right)\left(\frac{V_s^2}{V^2} - 1\right) \tag{4}$$

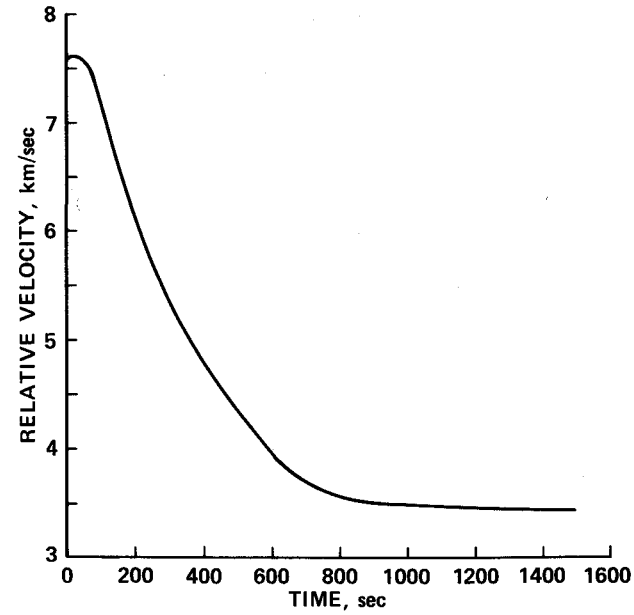

Fig. 3 Atmospheric braking trajectory on arrival at Mars at inertial velocity of 7.8 km/s and at an entry angle of −7.7 deg at 90 km.

The undershoot boundary, for a given deceleration a/g in Mars g, is defined by

$$\rho_{un} \approx \frac{2}{R_o}\left(\frac{m}{C_D A}\right)\frac{(V_s/V)^2(a/g)}{[1+(L/D)^2]^{1/2}} \tag{5}$$

The approximate width of the atmospheric corridor is the difference between the altitudes determined from Eqs. (4) and (5), although the velocities are not usually the same at the two boundaries. As can be seen from Eqs. (4) and (5), the overshoot boundary is highest when the maximum value of C_L is used and the undershoot boundary is lowest for the minimum value of C_D, all other factors being equal. Because the lowest value of C_D corresponds to $C_L = 0$, it is usually not possible to attain the theoretical minimum undershoot altitude, because shallow-angle flight cannot be maintained for any length of time without lift.

The influence on the corridor size of the entry vehicle shape is determined by comparing the aerodynamic characteristics of the winged configuration proposed here with those of blunted, raked-off, conical, or elliptic bodies[4] which have L/Ds of about 0.5. The maximum usable lift coefficients of the blunted bodies is about 0.65, whereas the winged vehicle can achieve a value of about 0.85. Assuming that the values of m/A for all of the configurations are the same, a 2.3-km-higher overshoot boundary is found for the winged vehicle. It is at the deceleration-limited undershoot boundary, however, where the winged vehicle's advantage is most pronounced. For example, the product $C_D[1 + (L/D)^2]^{1/2}$ appearing in the denominator of Eq. (5) is only about 0.14 as large for the winged shape as for blunted raked-off bodies at maximum L/D, which yields an 18-km-lower undershoot boundary for the winged vehicle. Of course, only a portion of the 18-km increase in the atmospheric corridor may be usable, since aerodynamic heating limitations must also be considered in defining the undershoot boundary.

The winged vehicle can also use aerodynamic control surfaces to maneuver within the atmosphere. The use of flaps to control the pitch and roll of blunt bodies requires a very complex design. The alternative is to use reaction controls that can consume several thousand kilograms of fuel during the 10-min deceleration pass. The modulation of the L/D that is required to fly the trajectory in Fig. 2 is shown in Fig. 4. To assure atmospheric capture when making shallow low-deceleration entries at hyperbolic speeds, negative lift must be used, as can be seen from Eq. (4). A maximum (absolute value) L/D of about 0.8 is required. (At an altitude of 44 km, the vehicle maximum L/D is over 2 at an angle of attack of about 17 deg.[8]) Precise modulation of the lift is necessary to assure a

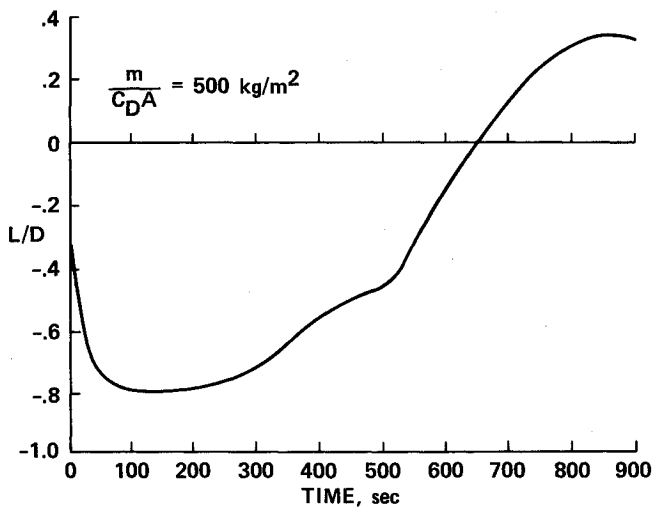

Fig. 4 Required modulation of lift-to-drag ratio for atmospheric capture trajectory shown in Figs. 2 and 3.

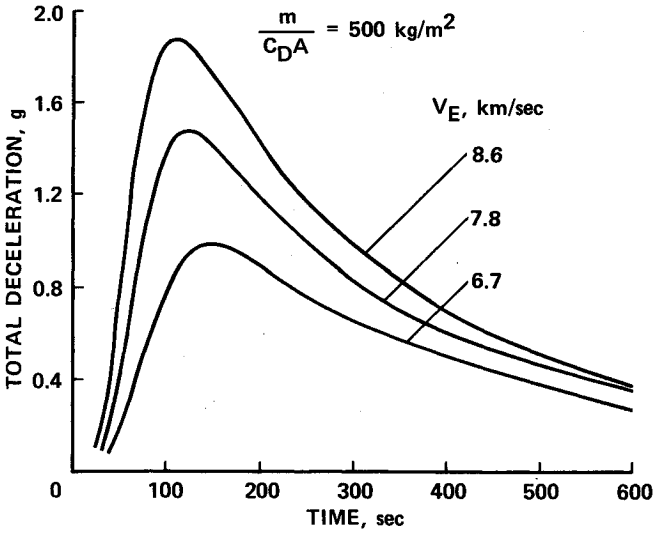

Fig. 5 Variation of total deceleration in Earth g during atmospheric braking.

low deceleration rate without skipping out of the atmosphere at too high a speed.

The total deceleration loads felt by the crew are shown in Fig. 5 for entry speeds of 6.7 and 8.6 km/s in addition to the 7.8 km/s entry trajectory previously discussed. The peak values occur between 110 and 150 s after entry and range from 1 to about 1.9 Earth g. Since the maximum deceleration during the descent from circular orbit was shown to be less than 1 Earth g in Ref. 8, the entire Mars atmospheric braking and the subsequent landing maneuver can therefore be performed at benign deceleration levels.

Heating Rates

The heating will be evaluated at the vehicle stagnation point, at a point on the wing leading edge and on the windward surface centerline. Only convective heating is important for the winged configuration in the speed range of interest here. However, the radiative heating will also be calculated at selected flight conditions and will be discussed subsequently. The convective stagnation point heating will be calculated using the correlation shown in Ref. 11, which gives (in W/cm^2)

$$\dot{q}_{w_0} = 1.35(10^{-8})(\rho/r_n)^{1/2}V^{3.04}\,[1 - h_w/H] \tag{6}$$

A comparison of Eq. (6) with shock tube and ballistic range data[11] showed good agreement to an equivalent flight speed of 10 km/s. Note that the stagnation-point convective heating rates in CO_2 are only about 5–6% higher than the rates in air over the velocity range of interest here.

The heating of the wing leading edge will be calculated using finite-length, swept cylinder theory in the form of

$$\dot{q}_{w_{LE}} \approx \left(\dot{q}^2_{w_{cyl}} + \dot{q}^2_{w_{FP}}\sin^2\Lambda_e\right)^{0.5} \tag{7}$$

where $\dot{q}_{w_{cyl}}$ is given by (in W/cm^2)

$$\dot{q}_{w_{cyl}} = 0.955(10^{-8})\left(\frac{\rho}{r_n}\right)^{1/2}V^{3.04}$$

$$\times(1 - 0.2\sin^2\Lambda_e)(\cos\Lambda_e)\left(1 - \frac{h_w}{h_{aw}}\right)$$

and

$$h_{aw} = h_\infty + (1 - 0.2\sin^2\Lambda_e)\frac{V^2}{2} \tag{8}$$

where $\sin\Lambda_e = \sin\Lambda\cos\alpha$. In Eqs. (7) and (8), Λ_e is the effective leading-edge sweep angle at angle of attack. The flat plate

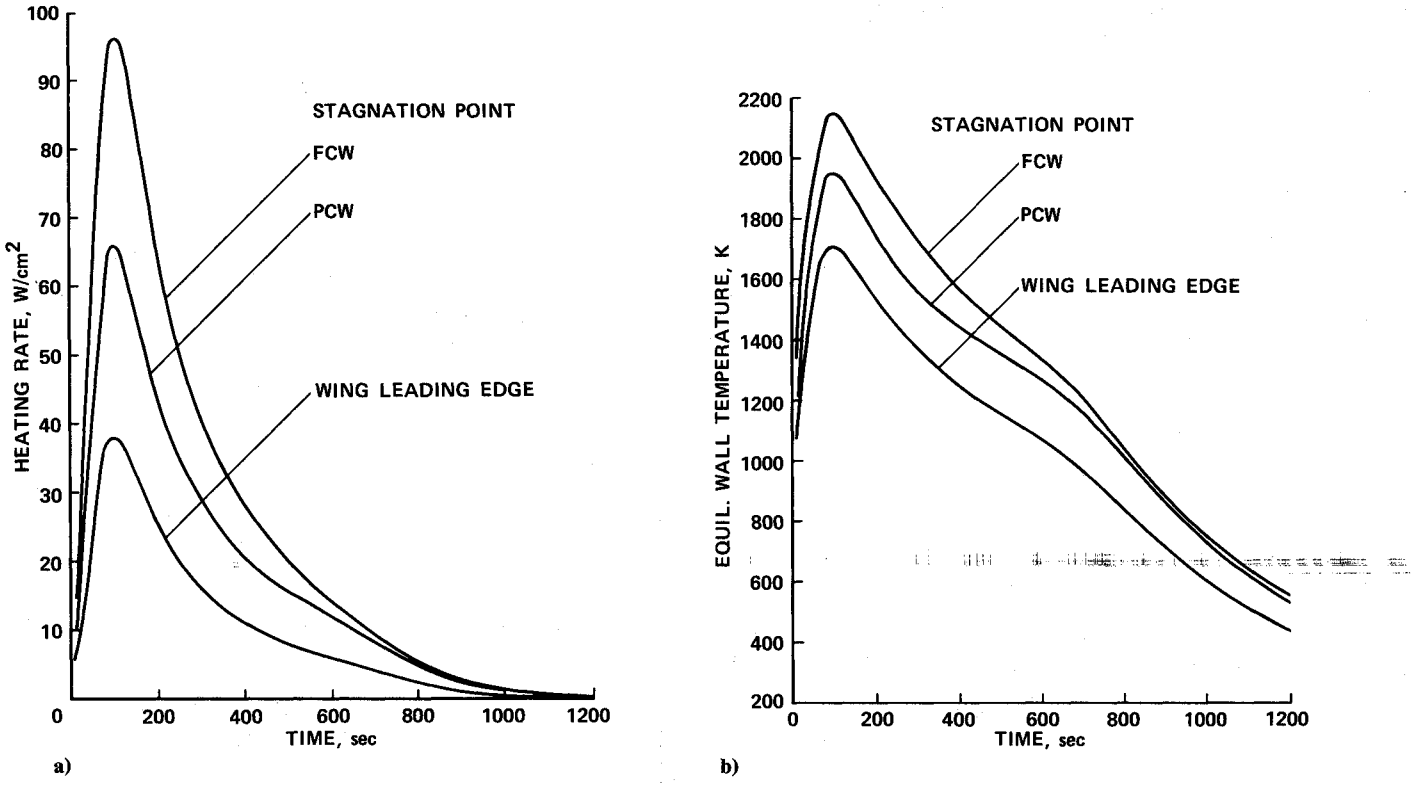

Fig. 6 Stagnation point and wing leading-edge heating during atmospheric braking from 7.8 km/s: a) heating rates; b) equilibrium wall temperatures.

heating contribution in Eq. (7), $\dot{q}_{w_{FP}}$, can be laminar, transitional, or turbulent. The laminar inclined-flat-plate heating expression is (in W/cm^2)

$$\dot{q}_{w_{FP}} = 1.87(10^{-9})(\rho \cos\delta_{FP}/x)^{1/2} \times V^{3.24} (\sin\delta_{FP})(1 - h_w/h_{aw}) \quad (9)$$

where δ_{FP} is the wedge angle, or angle of attack of the plate. For the wing leading edge, $\delta_{FP} = 90$ deg $- \Lambda_e$. For turbulent boundary-layer heating, expressions derived for air are used. These expressions are listed and applied in Ref. 12. Boundary-layer-transition correlations for air are used in the form presented in Ref. 13, but were modified to include transition information from Shuttle flights. The length of the transitional flow region is taken to be the same as the preceding laminar flow. In the heating relations described above, the boundary-layer-edge conditions were correlated in terms of flight condition and body surface slopes to facilitate application of the equations. The transport properties of Ref. 14 were used in the computations. All heating calculations will be made assuming that the inviscid shock layer flow is in equilibrium.

The heating given by Eqs. (6), (8), and (9) is based on the assumption that the vehicle surface is fully catalytic to atomic and molecular recombination. However, the high-speed heating can be significantly reduced when the surfaces are not fully catalytic, as was found in the case of the Shuttle Orbiter.[15] Paul Kolodzief of NASA Ames has recently computed catalytic reaction curves for several representative flight conditions in a CO_2 atmosphere. His results for a catalytic efficiency of 0.01 were incorporated in the present laminar boundary-layer computations and the effect on the heating of assuming partial wall catalycity will be illustrated. Because no significant heating reduction due to finite wall catalysis has been observed in turbulent boundary layers, the effect was not applied in regions of the vehicle that experienced turbulent flow. Catalytic wall effects will also be neglected in computing the wing leading edge heating, since the large sweepback reduces the shock-layer temperatures to levels where little dissociation occurs along most of the leading edge.

The stagnation point radiative heating will be calculated at several high-speed flight conditions to determine the importance of this heat transfer mechanism. The source of most of the radiative heating at the Martian entry speeds considered here is the CO molecule.[16] Although it is a potent radiator, the CN molecular concentration is so small in comparison with CO, based on calculations using an updated version of the code described in Ref. 17, that the CN contribution to the radiative heating is small.

It is advantageous to cool vehicles radiatively when large lifting surface areas such as the configuration proposed here are used. Although radiatively cooled surfaces require extensive insulation to protect the vehicle structure, very lightweight insulators are being developed.[18] Ablative heat shields tend to be heavy and become inefficient when heating rates are low. In addition, most ablators still require back-face insulation. Also, ablation usually produces rough surfaces. Roughness in the vicinity of the stagnation region where the boundary layer is thin can trigger transition, which increases the heating greatly downstream. During the Mars mission, the vehicle is only subjected to two heating pulses, unlike the Shuttle Orbiter that is designed for 40–50 flights. The first heating pulse is intense, but relatively brief, as the vehicle decelerates to satellite speed. The second pulse can last much longer, but the intensity is much milder, with the peak stagnation point wall temperature being under 1300 K.[7] Therefore, an upper limit for the heat shield temperature of about 2200 K should be sustainable for several minutes. The corresponding upper limit on the heating rate is about 106 W/cm^2 for a conservative

surface emissivity value of 0.8, which is used throughout the study.

The heating rates and the equilibrium wall temperatures were calculated for the 7.8 km/s entry velocity at the stagnation point and a representative location on the wing leading edge. A vehicle nose radius of 0.9 m is used and the wing leading-edge point is located 5 m from the fuselage, where the radius of the leading edge is 0. 18 m. As is shown in Fig. 6a, the heating rates peak about 100 s after entry and vary from 97 W/cm^2 for the fully catalytic surface (FCW) to 66 W/cm^2 for the partially catalytic wall (PCW). For the leading-edge point, the maximum heating rate is 39 W/cm^2. As previously mentioned, there is very little dissociation of the shock layer gas at the leading edge, since the shock layer temperature is only 2100 K at peak heating. Therefore, surface catalycity does not affect the wing leading-edge heating significantly. Note that the half-width of the heating pulses is only about 3.5 min. The equilibrium wall temperatures are presented in Fig. 6b. The peak value is 2150 K for the fully catalytic stagnation point. The partially catalytic stagnation point value is 1950 K, and

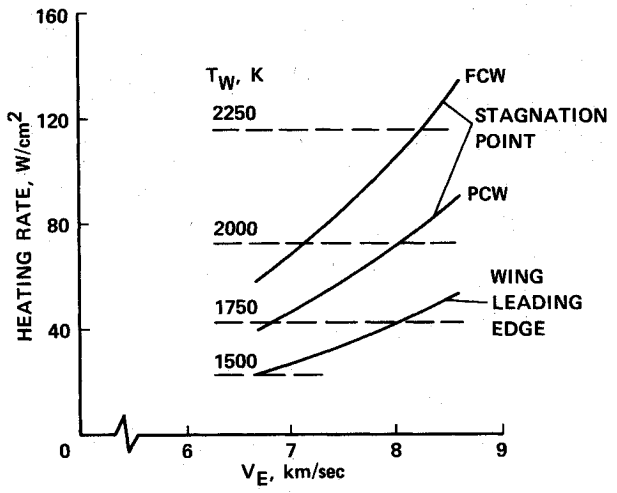

Fig. 7 Peak heating rates for low-deceleration trajectories.

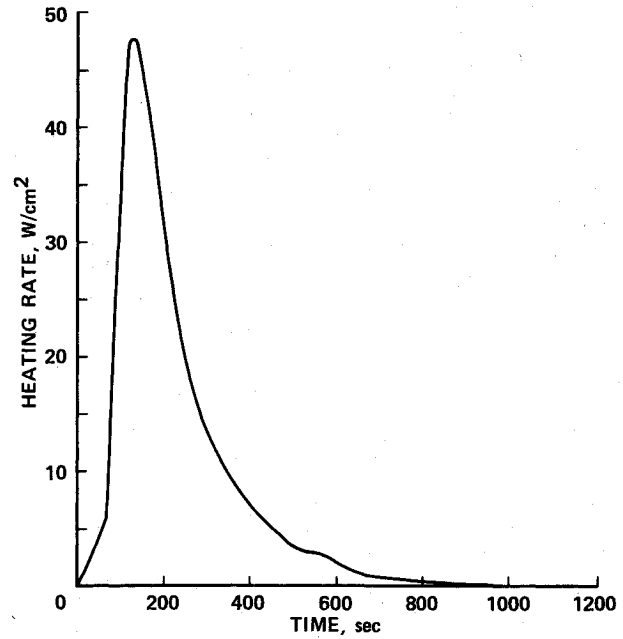

Fig. 8 Windward surface centerline point (x = 15 m) heating rates at 30-deg angle of attack.

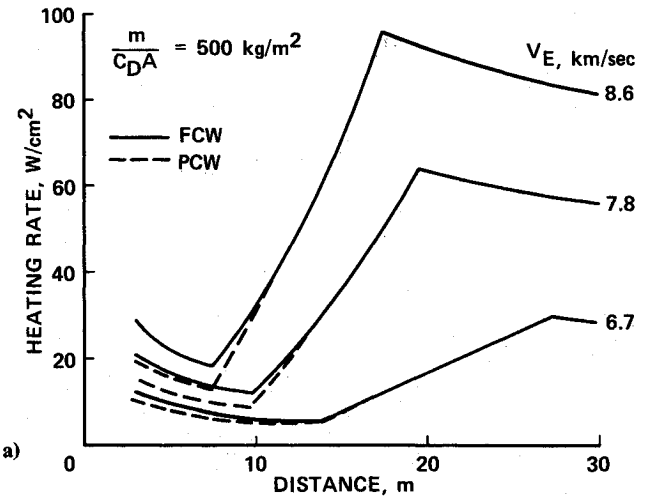

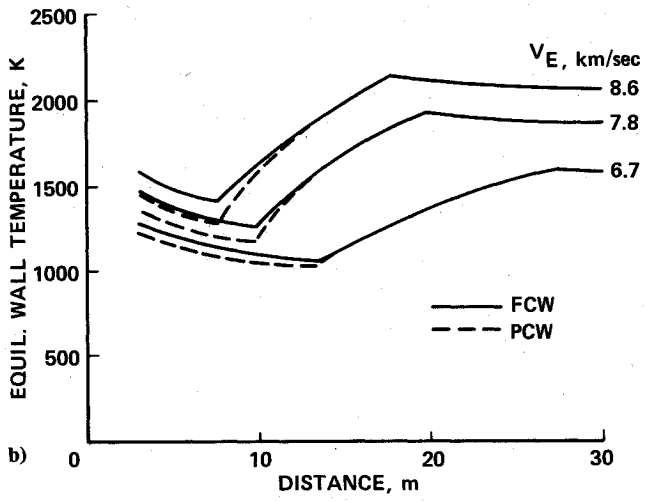

Fig. 9 Windward surface centerline heating distribution 100 s after entry at 30-deg angle of attack: a) heating rates; b) equilibrium wall temperatures.

the wing leading-edge temperature peaks near 1700 K. These values are below the previously stated temperature limit.

The peak heating rates experienced at the stagnation point and at the wing leading-edge point are shown in Fig. 7 as a function of entry velocity for the trajectories represented in Fig. 5. Note that the stagnation point can be radiatively cooled, even if the surface is fully catalytic, to an entry velocity of 8 km/s and to speeds greater than 8.6 km/s if the wall is partially catalytic. However, only convective heating rates are presented in Fig. 7, and it is important to determine the extent to which radiation increases the stagnation point heating. The radiative heating was computed for the 7.8 and 8.6 km/s entry trajectories and found to be 9 and 17 W/cm^2, respectively. Therefore, the radiative heating was only about 9 and 12% of the fully catalytic peak convective-heating rate near the overshoot boundary. However, because the radiation can peak several seconds prior to the convection, the maximum values are not necessarily directly additive. An important question is the influence of body shape and nose radius on the relative contributions of the convective and radiative heating, because the preceding values are for a vehicle with a nose radius of only 0.9 m. Therefore, two cases were also computed

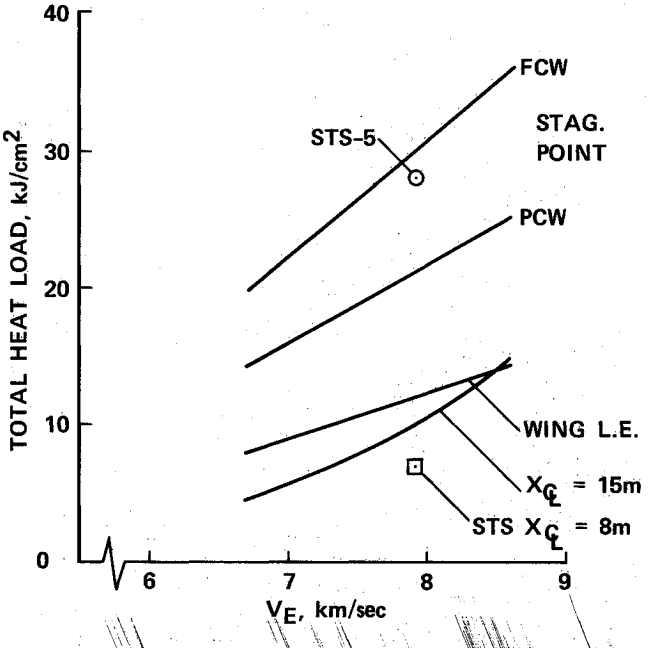

Fig. 10 Variation of total heat load with entry speed.

for raked-off cones with large nose-bluntness and having low L/D. A 7.8 km/s entry of a body with a 5-m nose radius, a peak $L/D = 0.3$, and $m/C_DA = 100$ kg/m^2 was calculated. It was found that the peak fully catalytic convective heating was 18.3 W/cm^2 while the radiative heating was 6.6 W/cm^2. A second case was calculated for the same body, with a 10-m nose radius, and entering at 8.6 km/s. The peak catalytic stagnation-point convection and radiation were 32.2 and 33.6 W/cm^2, respectively. Therefore, very large blunt bodies flying low-lift trajectories can experience radiative heating intensities that are comparable to the convective heating. Because much of the radiation is in the ultraviolet part of the spectrum, self-absorption is very important and was accounted for in the preceding calculation. However, because the radiation was typically less than 1% of the flow energy, the nonadiabatic shock-layer cooling was small.

Because the vehicle flies at an angle of attack of 30 deg during the atmospheric deceleration period, the windward surface can experience high heating rates. This observation is illustrated in Fig. 8, where the heating pulse is shown at the midpoint (15 m) on the windward centerline. The maximum value is almost 48 W/cm^2 and the pulse has a half-width of about 2.5 min. The corresponding equilibrium wall temperature peaks at 1800 K. The heating rate distribution along the vehicle centerline is illustrated in Fig. 9a for all three entry velocities. The rates shown in Fig. 9a occur 100 s after entry and represent the approximate peak values for turbulent flow. Note that the heating on the aft portion of the bottom surface is caused by turbulent flow and reaches values of approximately 60 W/cm^2 for the 7.8 km/s entry velocity and over 90 W/cm^2 for the 8.6 km/s case. The respective equilibrium wall temperatures (see Fig. 9b) are about 1900 K and over 2100 K. However, such high temperatures occur only briefly, and the total heat loads do not become excessive, as will be shown next.

Total Heat Loads

The major factor that determines the total heat shielding weight for a radiatively cooled vehicle is the total heat load. The total heat loads for the winged vehicle are presented in Fig. 10 as a function of entry speed. The heat loads are shown at the stagnation point, the wing leading-edge point, and the midpoint along the fuselage centerline. Only convective heating has been considered at the stagnation point. Because the radiative heating pulse is much shorter than the convective pulse, the contribution of radiation to the total heat input is essentially negligible over the speed range considered. In contrast, changing the wall catalycity can introduce about a 30% variation in the stagnation point heat load. In fact, the partially catalytic heat load is about 25% less than the heat input experienced during Shuttle Flight No. 5. The wing leading-edge heat loads are approximately half of the stagnation point values. The windward centerline-point heat loads rise rapidly with entry speed, because the occurrence of boundary-layer transition results in large increases in heating, as was shown in Fig. 9a. In comparison, the Shuttle centerline total heat load value[19] is about 30% lower, because, at the location shown, boundary-layer transition occurs late during the entry, when heating rates are low.

Concluding Remarks

It has been shown that a high-lift, winged vehicle will be able to use atmospheric braking very effectively to decelerate at least 5 km/s upon arrival at Mars. Following a nearly constant altitude deceleration period, the vehicle performs a skipping maneuver out of the atmosphere and goes into a low planetary orbit. For an entry speed of 7.8 km/s, the atmospheric braking period will last about 10 min with a peak deceleration that could be held as low as 1.5 Earth g. Precise lift modulation is necessary to assure atmospheric capture; an L/D exceeding 0.8 was required. It was shown that winged configurations potentially have much broader entry corridors than blunt, lifting shapes. Also, winged vehicles can use aerodynamic control surfaces to maneuver within the atmosphere, whereas blunt shapes most likely will use fuel-consuming reaction controls.

At an entry speed of 7.8 km/s, the peak heating rate will approach 100 W/cm^2 at the stagnation point for a fully catalytic surface. The corresponding equilibrium wall temperature was 2150 K. For a partially catalytic wall, the stagnation point, a representative wing leading-edge point, and the windward-surface centerline peak heating was about 40 to 65 W/cm^2, resulting in wall temperatures of under 2000 K. In fact, the vehicle could be radiatively cooled to entry speeds of over 8 km/s. The total heat loads at several body points were shown to be roughly comparable to values experienced during Shuttle entry. For the winged vehicle, radiative heating was found to be unimportant; however, finite-rate wall catalysis affected the stagnation point heating rates and total heat loads significantly. The combination of high-lift and effective modulation of the lift afforded by a winged configuration resulted in an efficient Mars atmospheric braking and surface descent vehicle.

References

[1]Syvertson, C. A., and Dennis, D. H., "Trends in High-Speed Atmospheric Flight," presented at the AIAA First Annual Meeting and Technical Display, Washington, DC, July 1964; NASA TM-X-54, 062.

[2]Tauber, M. E., and Seiff, A., "Optimization of Heating of Conical Bodies Making Lifting Hyperbolic Entries into the Atmospheres of Earth and Mars," *Proceedings of the AIAA Entry Technology Conference*, Williamsburg, VA, Oct. 1964.

[3]Clark, B., "Manned Mars Missions for the Year 2000," AIAA Paper 89-0512, Jan. 1989.

[4]Park, C., and Davies, C., "Aerothermodynamics of Manned Mars Missions," AIAA Paper 89-0313, Jan. 1989.

[5]Deerwester, J. M., and D'Haem, S. M., "Systematic Comparison of Venus Swingby Mode with Standard Mode of Mars Round Trip," AIAA Paper 67-27, Jan. 1967.

[6]*Planetary Flight Handbook*, "Part I—Speed Contours and Auxiliary Graphs for Manned Missions to Mars and Venus," NASA SP-35, 1963.

[7]Tauber, M. E., and Yang, L., "The Heating Environment During Martian Atmospheric Descent," AIAA Paper 88-2671, June 1988.

[8]Tauber, M. E., Bowles, J. V., and Yang, L., "Atmospheric Maneuvering During Martian Entry," AIAA Paper 88-4345, Aug. 1988.

[9]Eggers, A. J., Allen, H. J., and Neice, S. E., "A Comparative Analysis of the Performance of Long-Range Hypervelocity Vehicles,"NACA TR- 1382, 1958.

[10]Tauber, M. E., and Yang, L., "Performance Comparisons of Maneuvering Vehicles Returning from Orbit," *Journal of Spacecraft and Rockets,* Vol. 25, No. 4, 1988, pp. 263-270.

[11]Marvin J. G., and Deiwert, G. S., "Convective Heat Transfer in Planetary Gases," NASA TR R-224, July 1965.

[12]Tauber, M. E., and Adelman, H. G., "Thermal Environment of Transatmospheric Vehicles," *Journal of Aircraft*, Vol. 25, No. 4, 1988, pp. 355-363.

[13]Softley, E. J., Graber, B. C., and Zempel, R. E., "Experimental Observation of Transition of the Hypersonic Boundary Layer," *AIAA Journal*, Vol. 7, No. 2, Feb. 1969.

[14]Lee, J. S., and Bobbitt, P. J., "Transport Properties at High Temperatures of CO_2-N_2-O_2-Ar Gas Mixtures for Planetary Entry Applications," NASA TN D-5476, 1969.

[15]Rakich, J. V., Stewart, D. A., and Lanfranco, M. J., "Results of a Flight Experiment on the Catalytic Efficiency of the Space Shuttle Heat Shield," AIAA Paper 82-0944, June 1982.

[16]Woodward, H. T., "Predictions of Shock-Layer Radiation from Molecular Band Systems in Proposed Planetary Atmospheres," NASA TN D-3850, Feb. 1967.

[17]Menard, W. A., and Horton, T. E., "Shock-Tube Thermochemistry Tables for High-Temperature Gases," Jet Propulsion Lab., California Inst. of Technology, Pasadena, CA, TR 32-1408, Dec. 1969.

[18]Kourtides, D., and Pitts, W. C., "Flexible Heat Shield Technology," NASA TM-101071, Feb. 1989.

[19]Pitts, W. C., and Murbach, M. S., "Flight Measurements of Tile Gap Heating on the Space Shuttle," AIAA Paper 82-0840, June 1982.

James A. Martin
Associate Editor

Recommended Reading from the AIAA Progress in Astronautics and Aeronautics Series . . . AIAA

Thermal Design of Aeroassisted Orbital Transfer Vehicles

H. F. Nelson, editor

Underscoring the importance of sound thermophysical knowledge in spacecraft design, this volume emphasizes effective use of numerical analysis and presents recent advances and current thinking about the design of aeroassisted orbital transfer vehicles (AOTVs). Its 22 chapters cover flow field analysis, trajectories (including impact of atmospheric uncertainties and viscous interaction effects), thermal protection, and surface effects such as temperature-dependent reaction rate expressions for oxygen recombination; surface-ship equations for low-Reynolds-number multicomponent air flow, rate chemistry in flight regimes, and noncatalytic surfaces for metallic heat shields.

***TO ORDER:* Write, Phone, or FAX:** AIAA c/o TASCO, 9 Jay Gould Ct., P.O. Box 753, Waldorf, MD 20604 Phone (301) 645-5643, Dept. 415 ■ FAX (301) 843-0159

Sales Tax: CA residents, 7%; DC, 6%. For shipping and handling add $4.75 for 1–4 books (call for rates for higher quanties). Orders under $50.00 must be prepaid. Foreign orders must be prepaid. Please allow 4 weeks for delivery. Prices are subject to change without notice. Returns will be accepted within 15 days.

1985 566 pp., illus. Hardback
ISBN 0-915928-94-9
AIAA Members $49.95
Nonmembers $74.95
Order Number V-96